Progress In Electromagnetics Research C, Vol. 136, 215–227, 2023

Tumor Detection Using Microstrip Patch Antenna Operating in FCC MBAN Band

Satheesh Rao[1, 2, *], Ashish Singh[1], Anil K. Bhat[1], and Ramya Shetty[1]

Abstract—In this paper, a planar microstrip patch antenna operating in FCC MBAN for tumor detection is presented. The proposed antenna is constructed using a triangle-shaped patch with inset feeding. It is fabricated on an Arlon AD1000 substrate. Some of the parameters are assumed, and optimization is carried out to achieve greater performance. This prototype is placed on a human tissue mimicking model and simulated considering the cases of body model with tumor and without tumor. The designed antenna resonates at 2.37 GHz with 10 dB bandwidth of 3 MHz meeting the requirements specified by the FCC. Further, the introduction of a slot in the ground plane gives a half power beamwidth of 20.6° with directivity of 8 dB. This narrow beam is suitable for scanning application in microwave imaging. The fabrication of the antenna is carried out, and measurements are done to assess the performance of the antenna. Body phantom is created using petroleum jelly and mixture of wheat flour and water. The fabricated antenna is placed on the created model, and the variation in the resonant characteristics has been observed with the presence and absence of tumor.

1. INTRODUCTION

One of the largest causes for death worldwide is cancer. Detecting the malignant cell at an early stage will help in curing cancer. In today's scientifically advanced world, many advanced scanning devices such as MRI, CT scanner, and X-ray scanners are available. Using these scanners one can detect different health disorders such as tumor, melanoma, and kidney stones. The cost involved in such scans is huge. Further, these devices use ionized radiation. These ionized radiations are harmful to human body. Breast cancer is the most diagnosed cancer among women. Breast cancer cells usually form a tumor. Survival rates for breast cancer are very high provided that they are detected at an early stage. In economically poor countries it is expensive to detect and treat cancer. If a cost-effective screening device can be developed that uses non-ionized radiation, it will be very helpful in scanning such cancers at an early stage thereby reducing the death rate. A microstrip antenna-based scanning system can be a good alternative, and it can overcome the disadvantages of these commercial scanners.

An antenna is a metallic sensing structure which is used in converting electric signal into electromagnetic waves or vice versa. It is being widely used in communication systems [1–9]. Microstrip antenna is also helpful in patient monitoring, human body scanners, etc. which needs suitable tuning to a prescribed Medical Body Area Network (MBAN) band. Different types of microstrip antennas have been reported in the literature to scan human body for abnormal mass growth [10–17]. Various types of antennas for wireless communication and medical applications include phased array, defected ground structure (DGS), loading using notch and slot, different types of coupling, etc. [2–17]. The reported works in the papers show that there is ambiguity with respect to the frequency band to be used for medical applications. In 2014, Federal Communications Commission (FCC) recommended a

Received 1 July 2023, Accepted 9 August 2023, Scheduled 20 August 2023

* Corresponding author: Satheesh Rao (satheesh.rao@nitte.edu.in).

[1] Department of Electronics & Communication Engineering, NMAM Institute of Technology Nitte, Karnataka, India. [2] Research Scholar, Visvesvaraya Technological University (VTU), Belagavi-590018, Karnataka, India.

frequency band of 2.36 GHz–2.39 GHZ for indoor medical applications with 20 dB bandwidth of 5 MHz and a power of 1 mW.

In this article, a slot loaded equilateral triangle-shaped microstrip antenna having microstrip line feeding is proposed for the detection of tumor. The designed antennas resonate at 2.38 GHz and 2.375 GHz with 20 dB bandwidth less than 5 MHz having 99.5° & 20.6° half power beamwidth, respectively, suitable for biomedical scanning applications.

2. ANTENNA GEOMETRY

Figure 1 shows the triangular microstrip antenna which is fed by a microstrip line. This antenna has a square-shaped ground plane. The antenna 1 shown in Figure 1 has ground and substrate dimension of $(L \times W \times H)\,\text{mm}^3$ on which the radiating patch is equilateral triangle-shaped with side S_a mm. This antenna is fed by a microstrip line, and a 50 Ω SMA connector is used for excitation. To have a better impedance matching between patch and feed line, inset cuts are introduced into the microstrip patch. This modification gives rise to antenna 2 as in Figure 2 having a similar geometry to antenna 1. The dimension of the microstrip feed line is $(L_m \times W_m)\,\text{mm}^2$, and the inset dimension is $(L_i \times W_i)\,\text{mm}^2$. Figure 3 shows antenna 3, and the geometry of this antenna is the same as that of antenna 2, but this antenna has narrow radiation beam. To achieve narrow beam, a slot is introduced into the ground plane. The dimension of the slot is $(L_s \times W_s)\,\text{mm}^2$ with inset feed of antenna 2 retained as it is. The energization of this antenna is done using an SMA connector of 50 Ω impedance. Antenna 2 and antenna 3 are designed and fabricated on an Arlon AD1000 substrate having $h = 0.635$ mm of thickness. The designed antenna dimensions are as shown in Table 1. The fabricated microstrip antennas are as shown in Figure 4.

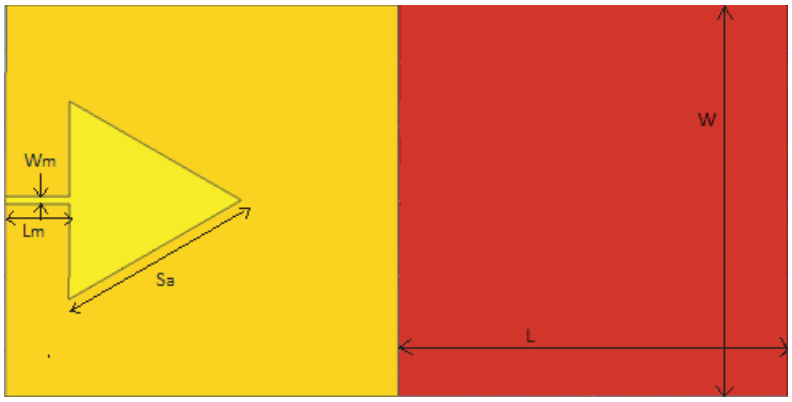

Figure 1. Antenna 1. (a) Front view, (b) back view.

2.1. Theoretical Analysis

To meet the FCC MBAN requirements for the application under consideration, a substrate with a higher dielectric constant is preferred. As a result, the design uses an Arlon AD 1000 substrate with a dielectric constant of 10.2. Based on formulae (1)–(4) [28], the radiating patch's size is determined.

$$f_{m,n} = \frac{2c}{3S_a\sqrt{\epsilon_{re}}}\sqrt{m^2 + mn + n^2} \tag{1}$$

For the case of TM_{10}, the value $m = 1$ and $n = 0$, and for more accuracy S_a is replaced with S_{ae}. Hence the resonance frequency is

$$f_{1,0} = \frac{2c}{3S_{ae}\sqrt{\epsilon_{re}}} \tag{2}$$

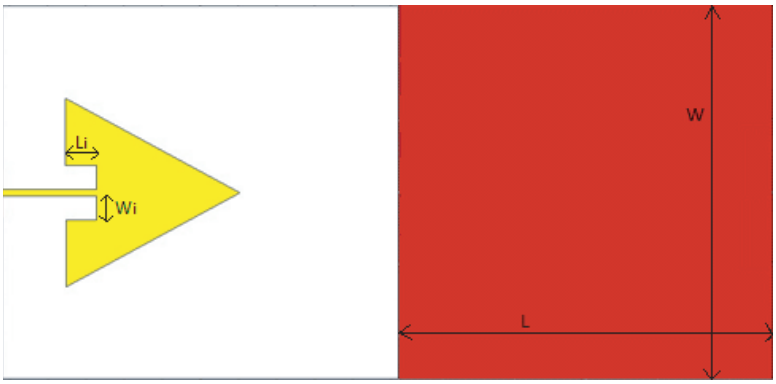

(a) (b)

Figure 2. Antenna 2. (a) Front view, (b) back view.

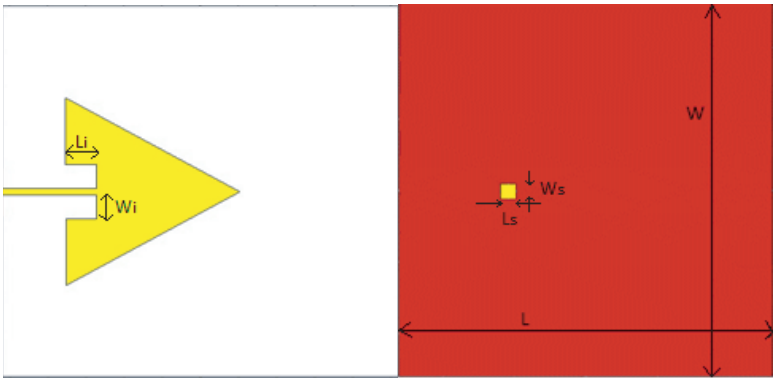

(a) (b)

Figure 3. Antenna 3. (a) Top view, (b) bottom view.

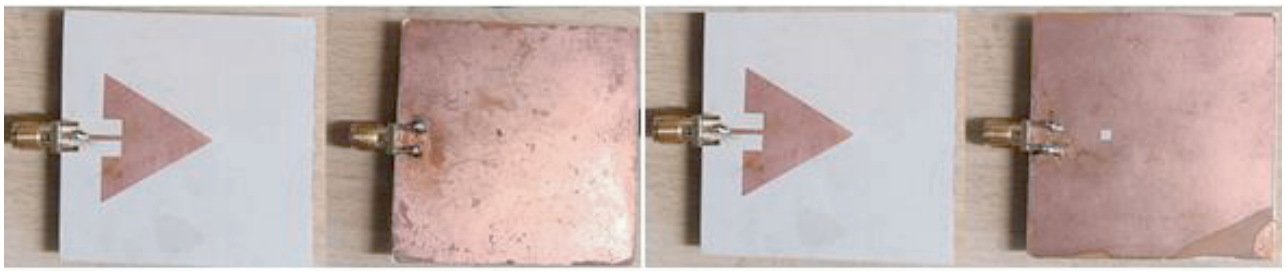

(a) (b)

Figure 4. Top and bottom view of fabricated, (a) Antenna 2 and (b) Antenna 3.

where the effective dielectric constant is

$$\epsilon_{re} = \frac{1}{2}\left[(\epsilon_r + 1) + (\epsilon_r - 1)\left(1 + \frac{12h}{w}\right)^{-\frac{1}{2}}\right] \tag{3}$$

and the effective side length of the equilateral triangle is

$$S_{ae} = S_a\left[1 + 2.199\frac{h}{S_a} - 12.853\frac{h}{S_a\sqrt{\epsilon}_{re}} + 16.436\frac{h}{S_a\epsilon_{re}} + 6.182\left(\frac{h}{S_a}\right)^2 - 9.802\frac{1}{\sqrt{\epsilon}_{re}}\left(\frac{h}{S_a}\right)^2\right] \tag{4}$$

Table 1. Dimensions of the designed antenna.

Parameter	Value (in mm)
L	52.506
W	52.506
S_a	26.35
W_m	1
L_m	12.42
W_s	2.05
L_s	2.05
W_i	3.3
L_i	4
h	0.635

The radio frequency (RF) equivalent R-L-C circuit for the triangular patch can be obtained by using a rectangular patch of the same area. The equivalent circuit is as shown in Figure 5. The values R-L-C are given as [29].

$$C_P = \frac{LW\varepsilon_0\varepsilon_{re}}{2h}\cos^{-2}\left(\frac{\pi X_0}{L}\right) \tag{5}$$

$$R_P = \frac{Q}{\omega_r C_P} \tag{6}$$

$$L_P = \frac{1}{\omega_r^2 C_P} \tag{7}$$

$$Q = \frac{c\sqrt{\varepsilon}_{re}}{hf_r} \tag{8}$$

L — Equivalent rectangular patch length; W — Equivalent rectangular patch width; h — Substrate thickness; ε_{re} — Effective dielectric constant of the substrate; X_0 — Feed point location along the length of the patch.

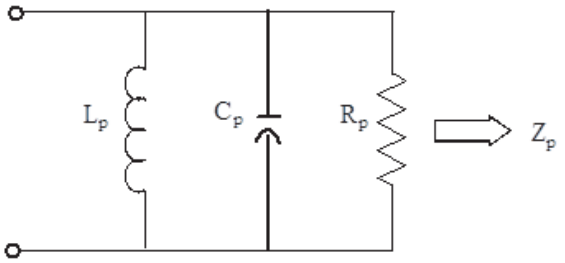

Figure 5. Equivalent network for patch.

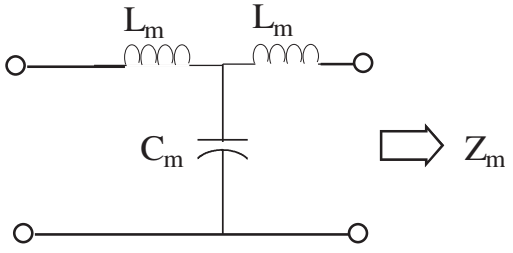

Figure 6. Equivalent network for microstrip feed line.

As illustrated in Figure 6, the microstrip feed line can be represented by an L-C circuit, and the values can be computed as [29]

$$L_m = 100h\left(4\sqrt{\frac{W_m}{h}} - 4.21\right) \text{ nH} \tag{9}$$

$$C_m = W_m(9.5\varepsilon_{re} + 1.25)W_m/h + 5.2\varepsilon_{re} + 7.0\} \text{ pF} \tag{10}$$

The impedance offered by the slot is Z_{Sl} and can be computed as [29],

$$Z_{Sl} = R_S + jX_S \tag{11}$$

$$R_{sl} = 60\left[C + \ln(kL_S) + \frac{1}{2}\sin(kL_S)\{S_i(kL_S) - 2S_i(kL_S)\} + \frac{1}{2}\cos(kL_S)\left\{C - \frac{\ln(kL_S)}{2} - C_i(2kL_S) - 2C_i(kL_S)\right\}\right]\cos(\Psi) \tag{12}$$

$$X_{sl} = 30\left[2S_i(kL_S) + \cos(kL_S)\{2S_i(kL_S) - S_i(2kL_S)\} - \sin(kL_S)\left\{2C_i(kL_S) - C_i(2kL_S) - C\left(2kW_S^2/L_S\right)\right\}\right] \tag{13}$$

where W_s — Slot width; L_S — Slot length; C — Euler's constant; Ψ — Slot inclination from radiating edge; k — Propagation constant and

$$S_i(x) = \int_0^x \frac{\sin(x)}{x}dx \tag{14}$$

$$C_i(x) = -\int_0^\infty \frac{\cos(x)}{x}dx \tag{15}$$

The slot's RF equivalent network is as shown in Figure 7.

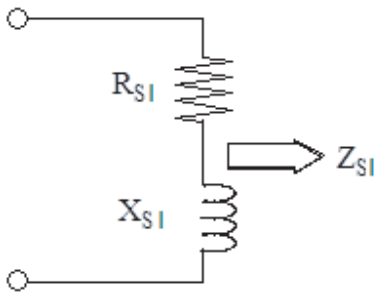

Figure 7. Equivalent network for the slot.

High frequency equivalent networks for the designed antenna 2 and antenna 3 are as shown in Figure 8. The networks effective impedance Z_{in} can be calculated using Equation (16) for antenna 2 and Equation (17) for antenna 3. The network's frequency of resonance can be computed using Equation (18). Equations (5)–(18) can be used to develop theoretical spice simulation model for the setup used.

$$Z_{in} = Z_p||Z_m \tag{16}$$

$$Z_{in} = Z_p||Z_m||Z_S \tag{17}$$

$$f_C = \frac{1}{2\pi\sqrt{LC}} \tag{18}$$

Different tissues or organs of the human body have different electrical properties such as conductivity, mass, and dielectric constant. The human body can be modelled using equivalent body capacitance C_{body} and body resistance R_{body}. When the designed antenna is placed over the human body, the antenna's equivalent impedance comes in parallel with the equivalent body network. The overall impedance of this network will decide the resonant frequency. Since the total impedance increases, the resonant frequency decreases. The tumors have different electrical properties as compared to normal tissues. They have higher dielectric constant and conductivity. When there exists tumor, the effective body capacitance will be greater, and hence there will be larger reduction in the resonant frequency, which is an indication for the presence of tumor. Figure 9 shows the high frequency equivalent network for the complete simulation setup.

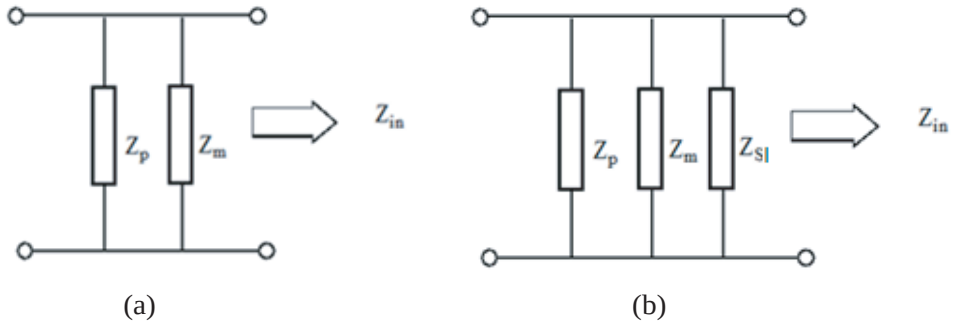

Figure 8. (a) RF equivalent network for antenna 2. (b) RF equivalent network for antenna 3.

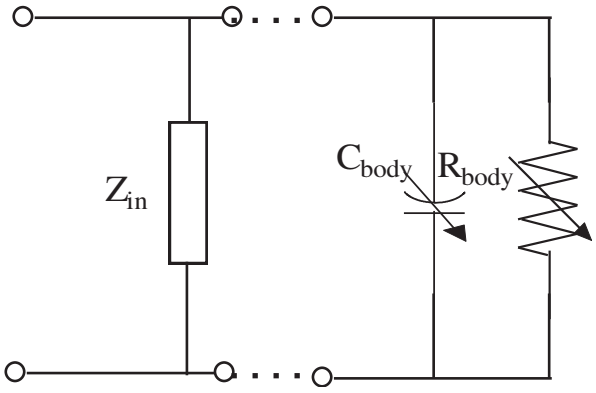

Figure 9. RF equivalent circuit for on body antenna placement [29].

3. RESULTS AND DISCUSSION

The equilateral triangular patch-based antenna named antenna 1 is designed on Computer simulation Technology (CST) studio for a resonant frequency of 2.37 GHz. The simulation result in Figure 10 shows that antenna 1 resonates at 2.363 GHz with reflection coefficient S_{11} of -4.43 dB. The large reflection is due to the mismatch between the antenna and the feed line impedance. Antenna 1 is modified to introduce the inset of dimension W_i and L_i to achieve a better match between feed line and the antenna that results in antenna 2 resonating at 2.383 GHz falling within the FCC MBAN band with reflection coefficient S_{11} of -31.618 dB which is well accepted. Their results are shown in Figure 10. The half power beamwidth of this antenna is 99.5°. Further, antenna 2 is modified by introducing a defect into the ground plane in the form of a slot loading leading to a new structure of antenna 3. The dimension of the slot is finalized based on the optimization of S_{11}. Due to the reactive loading introduced by the slot, the beamwidth of antenna 2 is reduced to 20.6°. Antenna 3 resonates at a frequency of 2.371 GHz with a reflection coefficient S_{11} of -23.94 dB. The presence of tumor can be detected using antenna 2 or antenna 3. However, reactive loaded antenna 3 is more suitable for scanning applications due to its narrow radiation beam. Both antenna 2 and antenna 3 frequency bands lie within FCC specified MBAN band. Computer simulation Technology (CST) Microwave Studio suite 2018 [16] has been used for designing and simulating the antennas.

The fabricated antennas are tested for reflection coefficient using Agilent PNA network analyzer, and the results are as shown in Figure 11. The measured results are seen to match the simulation ones; however, slight mismatch seen is due to the uneven fabrication process. Measured result shows that antenna 2 resonates at 2.4 GHz whereas antenna 3 resonates at 2.39 GHz. Table 2 shows the comparison of simulated and measured results.

To obtain better match between microstrip feed line and the patch, an inset cut is introduced. Figure 12 shows the effect of variation in the inset width on the reflection coefficient. It is observed

Table 2. Comparison of simulated and measured results.

	Resonant frequency (GHz)	
	Simulated	**Measured**
Antenna 2	2.3832	2.39
Antenna 3	2.371	2.4

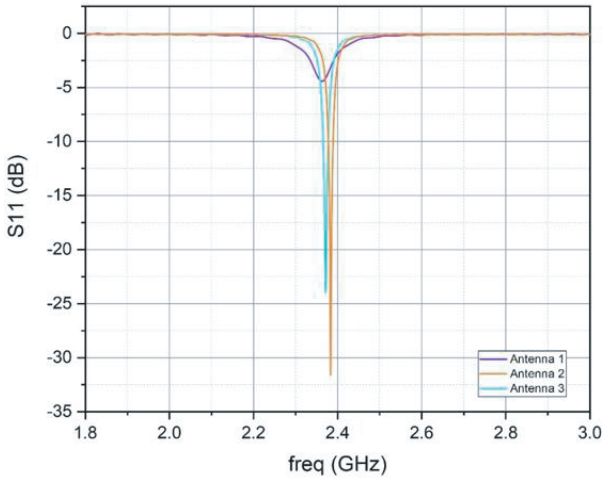

Figure 10. Reflection coefficients of Antenna 1, Antenna 2, and Antenna 3.

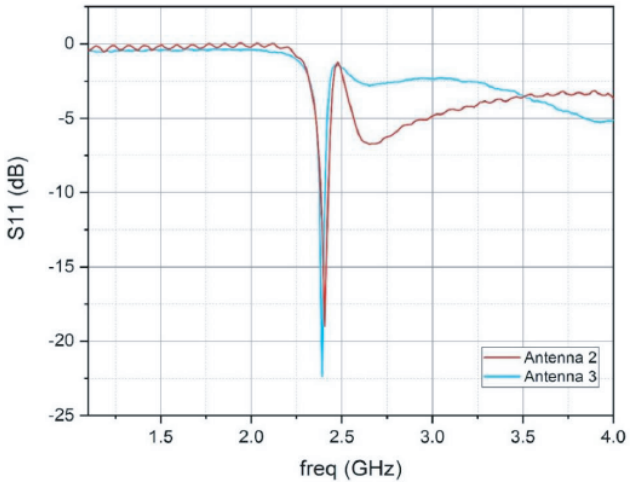

Figure 11. Measured results of Antenna 2 and Antenna 3.

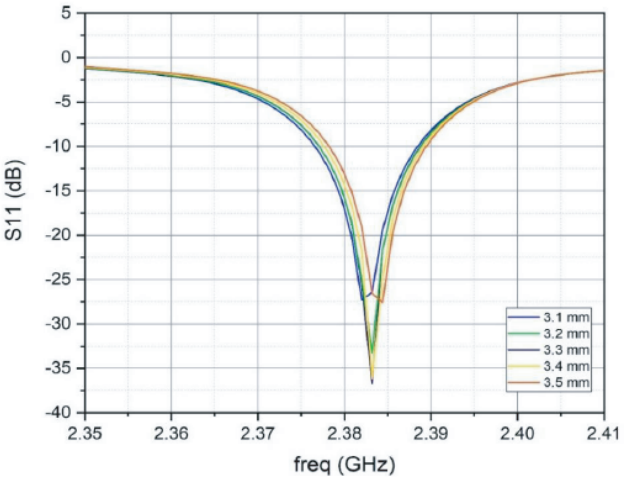

Figure 12. Variation of inset width W_i on reflection coefficient against frequency for Antenna 2.

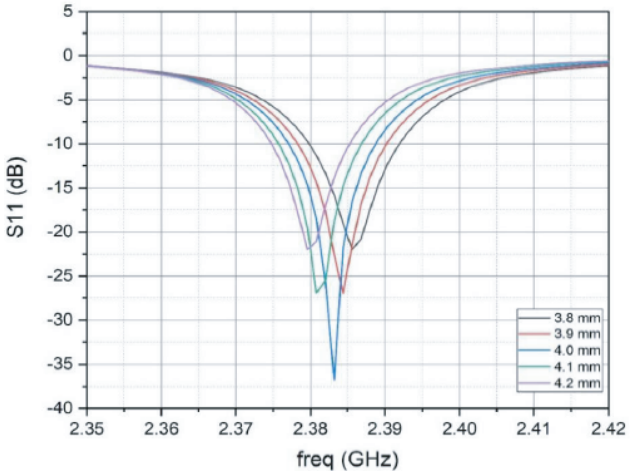

Figure 13. Variation of inset length L_i on reflection coefficient against frequency for Antenna 2.

that a good match is obtained for inset width equal to 3.3 mm. With increasing the length of the inset cut, variation in the reflection coefficient is observed. Figure 13 shows the results of cut length variation on the reflection coefficient. For inset length equal to 4 mm, the best match between patch and microstrip line is obtained. Inset cut length variation also shifts the resonant frequency due to the capacitance introduced by the inset cut. It is observed that with increasing and decreasing the

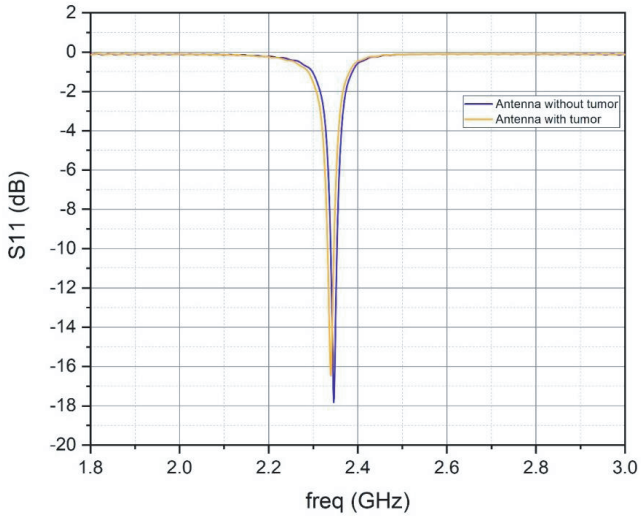

Figure 14. Simulated results of inset fed slot loaded ground plane with and without tumor.

(a) (b)

Figure 15. Measurement setup for testing fabricated antenna, (a) without tumor and (b) with tumor.

slot length L_i from 3.8 mm to 4.2 mm, shift in the resonant frequency is seen. As cut length increases, the resonant frequency decreases. This happens due to the change in reactance of resonator. A good match between the patch and feed line is achieved when inset length is 4 mm where reflection coefficient reaches a value of -38 dB.

A human body model is created on CST microwave studio, and the designed antenna 2 is mounted on this model. Simulation is carried out considering the body models with tumor and without tumor. The simulation results are as shown in Figure 14. Changes in the reflection coefficient and resonant frequency are observed. The reflection is higher with tumor, and the value is -16.46 dB whereas without tumor in the model, the observed reflection coefficient value is -17.82 dB. There also exists shift in the resonant frequency. Here, the antenna is used as a transmitting antenna, and the backscattered signals are captured and analyzed. Due to the higher dielectric property of the tumor, the effective body capacitance increases that leads to the decrease in the resonant frequency. The antenna without tumor

resonates at 2.34 GHz, and with tumor it resonates at 2.346 GHz. With a tumor, the resonance frequency is 6 MHz lower than that without tumor. Associated abnormal physiological or anatomical conditions along with the above result should be able to give a clue on the presence of tumor.

Figure 15 shows the experimental setup developed [27] to test the fabricated antenna with and without tumor. The fat layer of the human body model is constructed using petroleum jelly, and the tumor is modelled using wheat flour and water mixture. The electrical properties of these materials are as shown in Table 3. The fabricated antenna is placed on this model, and the reflection coefficients are measured for the antenna with tumor and without tumor. The test results are shown in Figure 16. It is noted that the reflection coefficient without body model is at −19.01 dB whereas with body model reflection coefficient moves up to −12.7 dB. There also exists shift in the resonant frequency from 2.39 GHz to 2.38 GHz. This is due to the change in dielectric property and is introduced by the body model. When antenna reflection coefficient is measured by inserting tumor, the reflection coefficient further moves up to −8.36 dB, and the resonant frequency shifts to 2.3 GHz. There is a shift of 0.8 GHz in the resonant frequency which is observed in the presence of tumor.

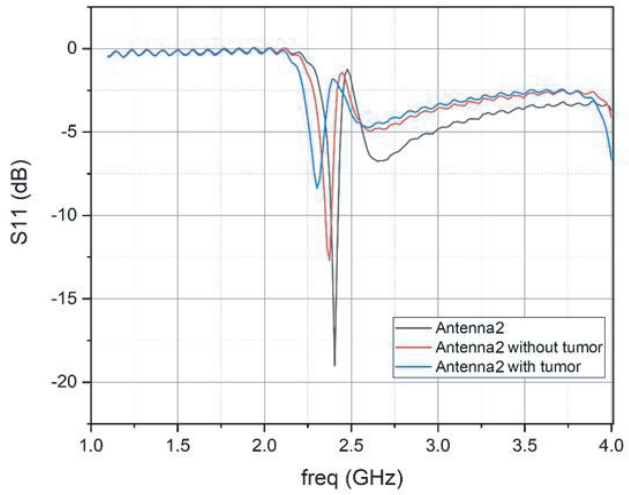

Figure 16. Measured reflection coefficient for antenna 2 without tumor and with tumor.

Table 3. Electrical properties of the material used [27].

Body model parts	Material used	Dielectric constant	Conductivity S/m
Fat	Petroleum jelly	2.36	0.012
Tumor	Wheat flour and water mix	28.1	1.32

3.1. Specific Absorption Rate (SAR)

SAR is a measure of the rate of RF energy absorption by the body from the source being measured in W/kg.

A body model is created on CST simulation software [16] using a skin layer of 1 mm thick, and the thickness of fat layer was 20 mm. Three tumor structures, each of 10 mm, were inserted into fat layer. The designed antenna is placed on this model, and simulation is carried out to measure SAR. Figure 17(a) indicates that on exposing body to the RF signal of 2.37 GHz frequency, the maximum SAR for 1 gm mass was 3.42149 W/kg. The maximum value was near the skin. It is also noted that there exists more absorption wherever there is tumor. In the simulation, 3 tumor models were inserted into the body model which is clearly seen in Figure 17(a). Figure 17(b) shows the SAR of only tumor

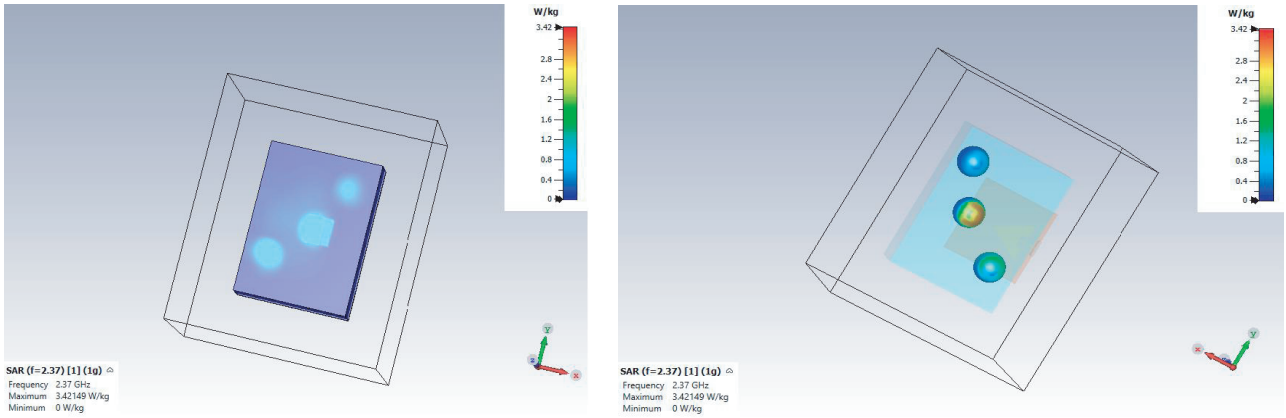

(a) (b)

Figure 17. (a) SAR for Antenna 2 — bottom view. (a) SAR for Antenna 2 — showing only tumor.

(a) (b)

Figure 18. (a) Voxel head model simulated on CST simulation tool [26]. (b) Voxel head model simulated on CST simulation tool [26].

to have a clear view. It is clear from Figure 17(b) that more absorption is seen in the tumor than other parts of the body.

To assess more information on effect of antenna field on human body, part of the Voxel head model has been utilized, and th eantenna is placed just above the head, as shown in Figure 18. Inn simulation, maximum electric field of 36378 V/m, magnetic field of 203.212 A/m, current density of 442.182 A/m^2 respectively were observed at 2.3832 GHz.

3.2. Current Distribution

The distribution of current on the surface of antenna 2 is as shown in Figure 19. The current flow on the patch is unidirectional indicating only one dominant mode. Maximum current density was 163.472 A/m seen at the perimeter of the radiating patch.

3.3. Radiation Pattern

The E-plane and H-plane patterns of triangular patch antenna 2 are as shown in Figure 20. E-plane pattern for $\theta = 0°$ is as in Figure 20(a). The 3 dB beamwidth is 89.9°. H-plane pattern for $\theta = 90°$ is as in Figure 20(b) with 3 dB beamwidth 103.9°.

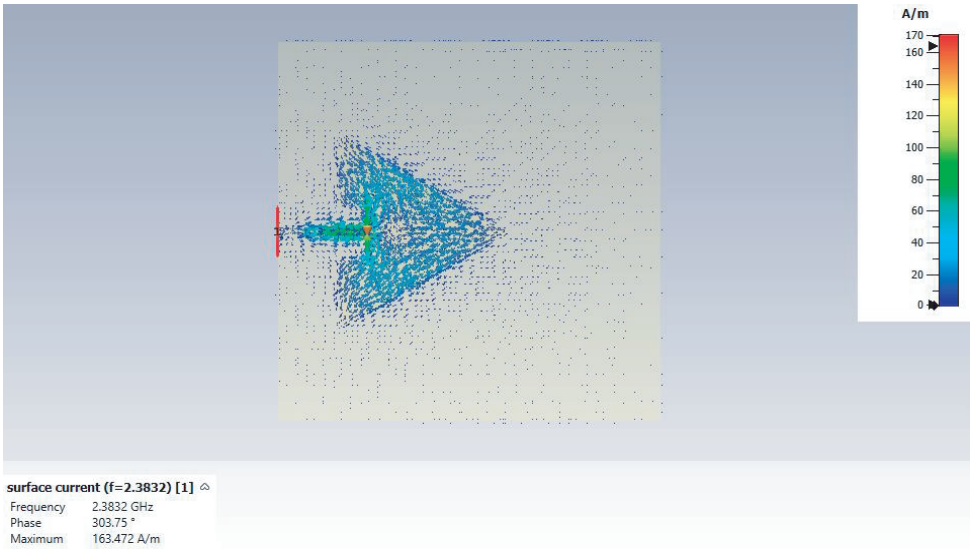

Figure 19. Current distribution of the antenna 2.

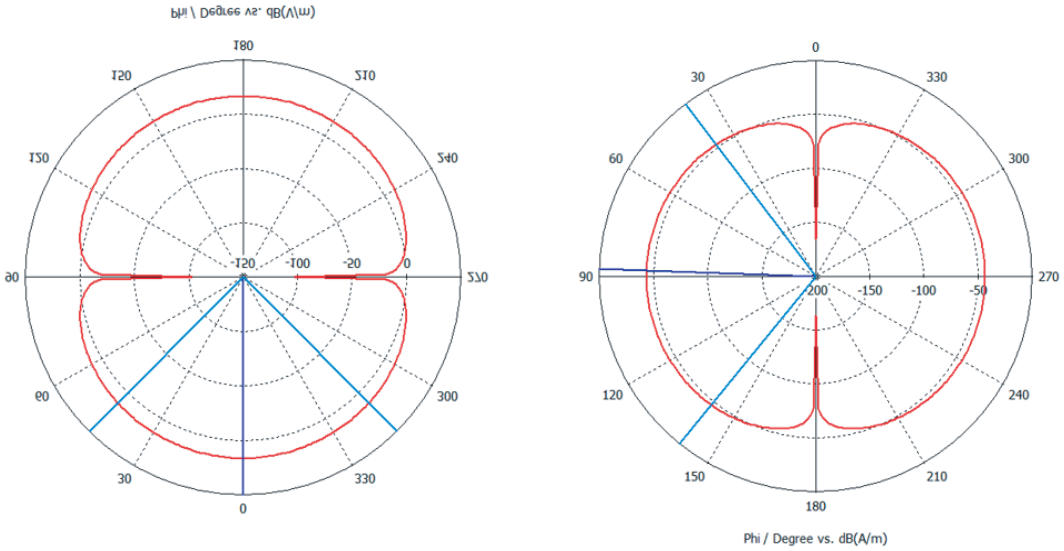

(a) (b)

Figure 20. (b) Radiation pattern of Antenna 2 at 2.3832 GHz — E Plane. (b) Radiation pattern of Antenna 2 at 2.3832 GHz — H Plane.

4. CONCLUSION

An equilateral triangle-shaped patch antenna for the application in biomedical field has been designed, tested, and presented. The paper also gives the theoretical analysis and high frequency equivalent model for both antenna and human body. Antenna 2 which resonates at 2.3832 GHz has been used in detecting the tumor. The simulation as well as test setup results shows that there exists considerable shift in the resonant characteristics in the presence of tumor. Hence, antenna 2 can detect tumors with great clarity. Future work can be done on improving the bandwidth of the antenna. Resonant characteristics of both the antennas lie in FCC MBAN. Antenna 3 characteristics observed at 2.371 GHz has shown very good radiation pattern with narrow beam, suitable for body scanning applications. This antenna can be used in body scanning applications wherein tumor, kidney stone, etc. can be detected.

REFERENCES

1. Chung, K. L. and C. H. Wong, "Wang-shaped patch antenna for wirless communication," *IEEE Antennas and Wireless Propagation Letters*, Vol. 9, 638–640, 2010.
2. Gosalia, K. and G. Lazzi, "Reduced size, dual-polarized microstrip patch antenna for wireless communications," *IEEE Transactions on Antenna and Propagation*, Vol. 51, 2182–2186, 2003.
3. Liang, Z., J. Liu, Y. Li, and Y. Long, "A dual-frequency broadband design of coupled-fed stacked microstrip monopolar patch antenna for WLAN applications," *IEEE Antennas and Wireless Propagation Letters*, Vol. 15, 1289–1292, 2016.
4. Elsadek, H. and D. M. Nashaat, "Multiband and UWB V-shaped antenna configuration for wireless communications applications," *IEEE Antennas and Wireless Propagation Letters*, Vol. 7, 89–91, 2008.
5. Li, P. K., Z. H. Shao, Q. Wang, and Y. J. Cheng, "Frequency-and pattern-reconfigurable for multistandard wireless applications," *IEEE Antennas and Wireless Propagation Letters*, Vol. 14, 333–336, 2015.
6. Minasian, A. A. and T. S. Bird, "Particle swarm optimization of microstrip antennas for wireless communication systems," *IEEE Transactions on Antennas and Propagation*, Vol. 61, 6214–6217, 2013.
7. Yang, F., X.-X Zhang, X. Ye, and Y. Rahmat-Samii, "Wide-band E-shape patch antennas for wireless communications," *IEEE Transactions on Antennas and Propagation*, Vol. 49. 1094–1100, 2001.
8. Bakariya, P. S., S. Dwari, M. Sarkar, and M. K. Mandal, "Proximity-coupled multiband microstrip antenna for wireless applications," *IEEE Antennas and Wireless Propagation Letters*, Vol. 14, 646–649, 2015.
9. See, C. H., R. A. Abd-Alhameed, D. Zhou, T. H. Lee, and P. S. Excell, "A crescent-shaped multiband planar monopole antenna for mobile wireless applicatons," *IEEE Antennas and Wireless Propagation Letters*, Vol. 9, 152–155, 2010.
10. Tak, J., S. Woo, J. Kwon, and J. Choi, "Dual-band dual-mode patch antenna for On/off-body WBAN communications," *IEEE Transactions on Antennas and Wireless Propagation Letters*, Vol. 15, 348–351, 2016.
11. Kissi, C., M. Särestöniemi, T. Kumpuniemi, et al., "Reflector-backed antenna for UWB medical applications with on-body investigations," *International Journal of Antennas and Propagation*, Vol. 2019, Article ID 6159176, 17 pages, 2019.
12. Nilavalan, R., I. J. Craddock, A. Preece, J. Leendertz, and R. Benjamin, "Wideband microstrip patch antenna design for breast cancer tumour detection," *IET Microwaves, Antennas & Propagation*, Vol. 1, 277–281, 2007.
13. Cheng, X., D. E. Senior, C. Kim, and Y.-K. Yoon, "A compact omni-directional self-packeged patch antenna with complementary split-ring resonator loading for wireless endoscope applications," *IEEE Transactions on Antennas and Wireless Propagation Letters*, Vol. 10, 1532–1535, 2011.
14. Conway, G. A. and W. G. Scanlon, "Antennas for over-body-surface communication at 2.45 GHz," *IEEE Transactions on Antennas and Propagation*, Vol. 57, 844–855, 2009.
15. Jofre, L., M. S. Hawley, A. Broquetas, et al., "Medical imaging with microwave tomographic scanner, *IEEE Trans. on Biomedical Engg.*, Vol. 37, 303–312, 1990.
16. Deeksha, B., A. Sai Ravi Teja, E. Sai Laxshmi, M. Nikhil Eshwar, and A. Singh, "Electromagnetically coupled notches loaded patch antenna for bio-medical applications," *IEEE conference IMPACT 2017, Aligarh University*, 283–286, 2017.
17. Bahl, I. J., S. S. Stuchly, and M. Stuchly, "A new microstrip radiator for medical applications," *IEEE Trans. on Microwave Theory and Techniques*, Vol. 28, No. 12, 1464–1469, Dec. 1980.
18. FCC, "Medical body area network measurement procedures," pub 670572D01MBANv01, 2015.
19. Bahal, I. J., *Lumped Elements for RF and Microwave Circuits*, Artech House, Boston, 2003.
20. Kumar, G. and K. P. Ray, *Broadband Microstrip Antenna*, Artech House, USA, 2003.

21. Bahal, I. J. and P. Bartia, *Microstrip Patch Antenna*, Artech House, 1980.
22. Singh, A., M. Aneesh, Kamakshi, and J. A. Ansari, "Analysis of microstrip line fed patch antenna for wireless communications," *Open Engineering*, Vol. 7, 279–286, 2017.
23. Singh, A., K. Shet, D. Prasad, A. K. Pandey, and M. Aneesh, "A review: Circuit theory of microstrip antennas for dual-multi- and ultra-widebands," *Modulation in Electronics and Telecommunications*, Intechopen, Book Chapter, 2020.
24. Balanis, C. A., *Antenna Theory, Analysis and Design*, 2nd Edition, Wiley, New York, 1997.
25. Terman, F. E., *Electronic and Radio Engineer*, 15, Kagakasha, Tokyo, Japan, 1995.
26. *Computer simulation Technology Microwave Studio Suite 2018*, 2018.
27. Alshehri, S. A., S. Khatun, A. B. Jantan, R. S. A. Raja Abdullah, R. Mahmood, and Z. Awang, "Experimental study of breast cancer detection using UWB imaging," *Proceeding of the International Conference on Advanced Science, Engineering and Information Technology, 2011*, 2011.
28. Bahl, I. J. and P. Bhartia, *Microstrip Antannas*, Artech House, USA.
29. Rao, S., A. Singh, A. K. Bhat, Durgaprasad, and K. Shet, "Reactively loaded stripline fed rectangular patch antenna for wireless and biomedical applications," *Progress In Electromagnetics Research C*, Vol. 128, 219–229, 2023.